Supporting information for

Cu^{1+} in HKUST-1: Selective gas adsorption in the presence of water

Nour Nijem,$ Hendrik Bluhm, * May L. Ng , * Martin Kunz, # Stephen R. Leone,$,* Mary K. Gilles*

$Departments of Chemistry and Physics, University of California Berkeley, CA 94720
#Advanced Light Source, Lawrence Berkeley National Lab, 1-Cyclotron Rd, Berkeley, CA, 94720
*Chemical Sciences Division, Lawrence Berkeley National Lab, 1-Cyclotron Rd, CA 94720

S1. Effect of sample activation and X-ray induced effects.

To characterize temperature and X-ray induced effects on the copper oxidation state in Cu$_3$(btc)$_2$ NEXAFS spectra were collected at two different activation temperatures (left) and x-ray irradiation times (right) (Figure S1). An increase in the Cu^{1+} peak is observed as the activation temperature is increased from 100 ^{o}C to 180 ^{o}C and as a result of X-ray induced reduction of Cu^{2+} to Cu^{1+}. Slight differences in both NEXAFS spectra are observed and are related to the origin of the copper reduction. Although in both cases the resulting oxidation state is similar, thermally induced reduction might result from defects caused by a missing linker,[1,2] while x-ray reduction results from an interaction of the low energy electrons with the material.[3]
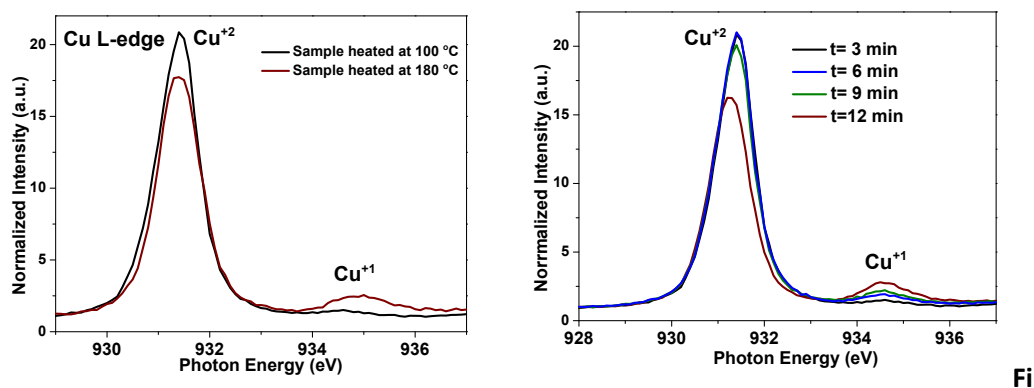
Figure S1. Cu L-edge NEXAFS spectra showing effect of activation temperature (left), and scan time on Cu oxidation state (right) in vacuum. The spectra are normalized to the pre-edge intensity.

The amount of Cu^{1+} present in the pristine HKUST-1 thin film was calculated from the Cu 2p$_{3/2}$ spectrum shown in the left panel of Figure S2. The right panel of Figure S2 shows the Cu 2p$_{3/2}$ spectrum in 0.2 Torr of NO. A new shake up (satellite) peak indicates a contribution from oxidized Cu^{1+}.[4]
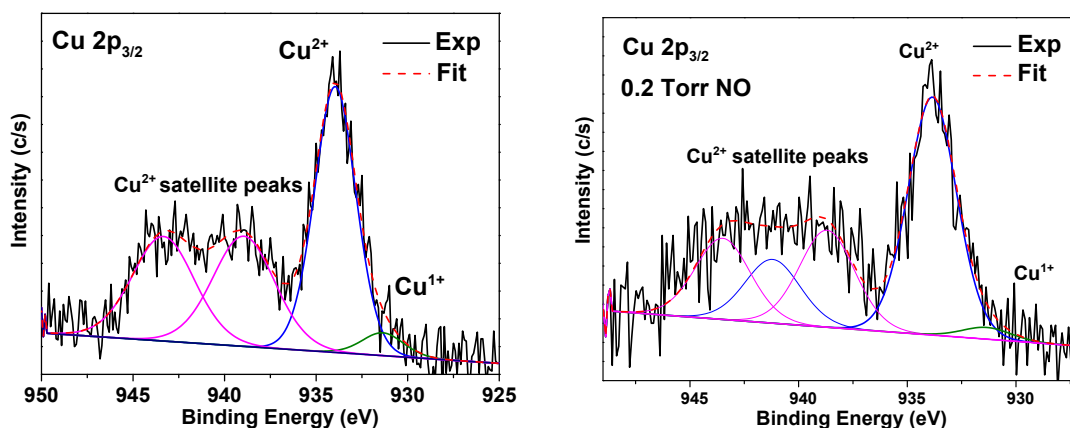
Figure S2. Left: Cu $2p_{3/2}$ photoelectron spectrum measured in UHV. Spectrum measured with an 1140 eV photon energy. Right: Cu $2p_{3/2}$ photoelectron spectrum measured in 0.2 Torr NO.

The spot size of the beam was ∼ 0.2 x 0.1 mm^2 in diameter with a photon flux of ∼1.5x10^{12} photons/second. To control X-ray exposure, a fresh spot was used to record XPS and NEXAFS spectra. Prior to experiments for each film, the film homogeneity was confirmed by measuring C 1s spectra (shown in Figure S3), at four different sample locations.
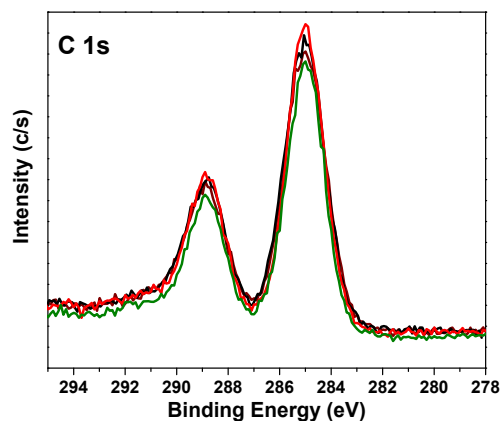
Figur

e S3. C 1s XPS spectra at four different sample locations on the thin film showing homogeneous coverage. Spectra measured with 490 eV photon energy.

S2. Growth of HKUST-1 thin film on SiO$_2$ substrates using the layer-by-layer method.

Thin films (~100 nm thick) of Cu$_3$(btc)$_2$ were deposited at 22 °C on SiO$_2$ coated quartz crystal microbalance (QCM) substrates using the layer-by-layer approach for a total of 40 layers.[5] Figure S4 left: The mass uptake for the first three layers, the deposition starts with five minutes flow of Cu acetate on the SiO$_2$ surface followed by an ethanol rinse (10 min), then five minutes of the trimesic acid solution followed by an ethanol rinse (10 minutes), this cycle is repeated 40 times. Figure S4 right: grazing incidence x-ray diffraction patterns (chi=0.2°) for the bulk Cu$_3$(btc)$_2$ (black) and the thin film deposited on SiO$_2$ substrate (blue). The films show a preferential orientation with the {111} facet parallel to the layer's surface as expected for Cu$_3$(btc)$_2$ grown on an OH functionalized substrate.[5,6] Film thickness is calculated from the mass uptake and is estimated to be ~110 nm for 40 layers.
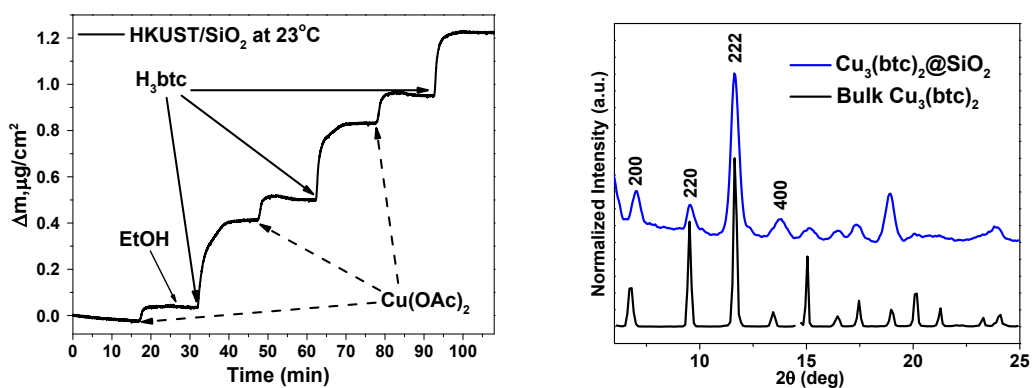
Figure S4. Left: Mass uptake of the Cu acetate (Cu(OAc)$_2$) and trimesic acid (H$_3$btc) in the layer-by-layer deposition, the layers are separated by an ethanol rinse; right: Grazing incidence (chi=0.05-0.5°) X-ray diffraction patterns of bulk Cu$_3$(btc)$_2$ (black) and 100 nm Cu$_3$(btc)$_2$ thin film deposited on a SiO$_2$ substrate (blue).

The activation of the thin films, removal of adsorbed water and solvent from the pores, for both the APPES and QCM measurements were performed by heating the sample overnight to 110 °C in vacuum (1x10^{-8} Torr).

S3. NO adsorption isotherm of HKUST-1 thin film measured using a gas phase based quartz crystal microbalance.

NO adsorption isotherm (Figure S5) shows an adsorption of 0.166 mmol/g (0.36 wt%) of NO at 0.3 Torr. This value corresponds to ~1 NO molecule per ~13 dicopper tetracarboxylate building blocks for $Cu_3(btc)_2$ at conditions similar to the APPES measurements .
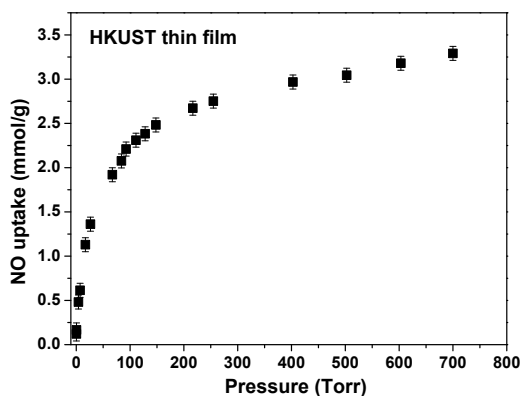
Figure S5. NO adsorption isotherm as a function of pressure for a 100 nm thick $Cu_3(btc)_2$ thin film at 298 K.

S4. Assignment of NO adsorbed at Cu^{1+} sites.

To assign the peaks associated with adsorbed NO, N 1s photoelectron spectra were collected at the same sample location for different scan times (beam exposure time). Figure S6 shows N 1s photoelectron spectra under ultra high vacuum UHV (bottom) with a scan time of 207 seconds and at 0.2 Torr with scan times of 92 and 207 seconds. The sharp spectral features are assigned to the NO gas phase overlapping with the adsorbed NO features. The adsorbed NO experiences charging effects, and is corrected using the measured position of the C 1s and scaling it to the known position (285 eV). The contribution of the gas phase species (peak area) varies depending on the volume of gas probed. This volume depends on the distance between the detector and the sample and changes slightly when different sample locations are probed. This allows for verification of these peak assignments. The integrated areas of the two NO species increased with increasing beam exposure time. Increases of ~24±30% for the 403.5 eV peak and ~171±30% for the 406 eV peak were observed. Figure S7 shows similar effects for spectra collected at 0.1 Torr NO at the same spot as a function of beam exposure time. The 406 eV peak is absent at 48 seconds of X-ray beam exposure, however, as the scan time is increased this peak appears. Therefore, we can assign the peak at 403.5 eV to NO adsorbed at the Cu^{2+} sites. As beam induced effects (photo-reduction of Cu^{2+}) take place, a new peak at 406 eV emerges, and is assigned to NO adsorbed at the Cu^{1+} sites.
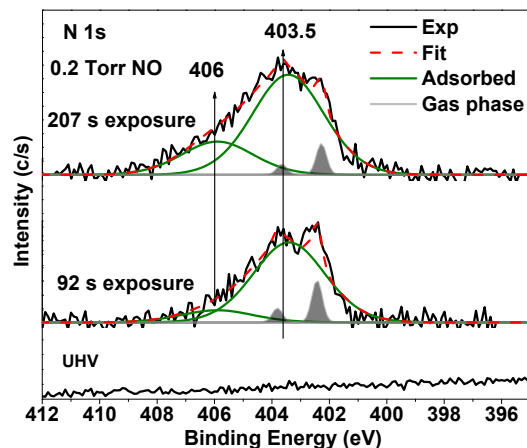
Figure S6. N 1s photoelectron spectra in UHV (bottom) with beam exposure of 207 seconds, 0.2 Torr NO for beam exposures of 92 (middle) and 207 seconds.
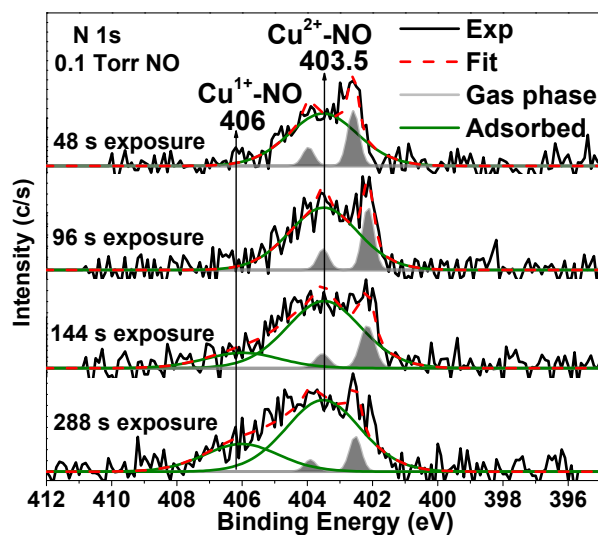
Figure S7. N 1s XPS spectra at 0.1 Torr NO as a function of x-ray exposure time. An increase in the 406 eV peak intensity occurs as X-ray exposure time increases.

The integrated areas of the N 1s peaks correlate to the amount of species present. With an increased beam exposure time at 0.2 Torr NO a two fold increase in the total integrated area of the 403.5 and 406 eV peaks is observed (Figure S8 (left)). This increase indicates the formation of new adsorption sites by induced photo-reduction of unoccupied Cu^{2+} metal centers, rather than a total conversion of the pre-adsorbed NO species. The right part of Figure S8 shows the behavior of the different NO species as a

function of exposure time. Both species increase with exposure time, indicating occupation of Cu^{2+} sites in the Cu^{2+}/Cu^{1+} dimers.
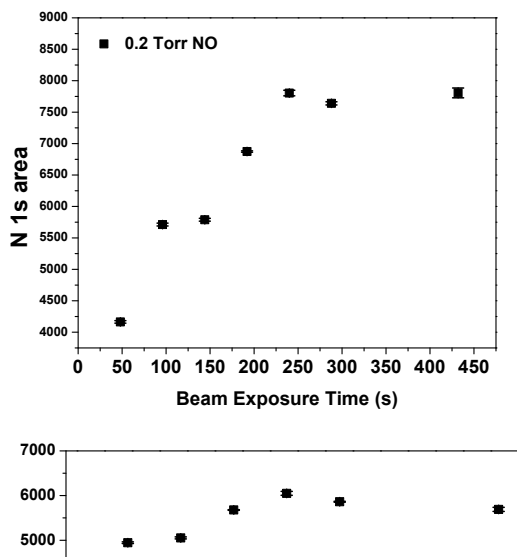
The Chemical integrity of the films is verified by recording C 1s and O 1s XPS spectra (Figure S9). The line shapes of the C 1s and O1s XPS spectra do not change which indicates the integrity of the framework is
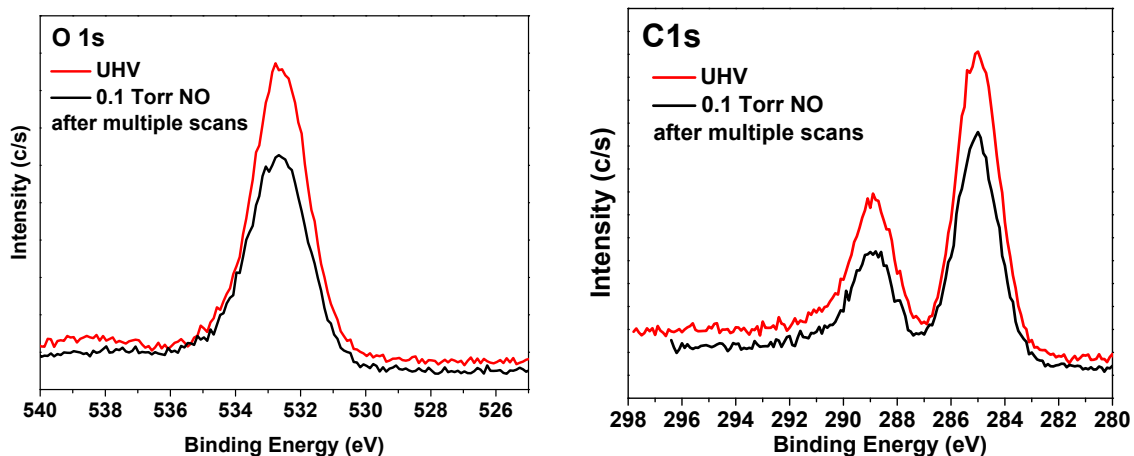
Figure S9. O 1s and C 1s XPS spectra in UHV (red) and at 0.1 Torr NO (black) after beam exposure for 288 seconds.

maintained (Figure S9, right). The structural integrity was verified by recording the X-ray micro-diffraction of both the original and x-ray exposed part of sample shown in Figure S10.
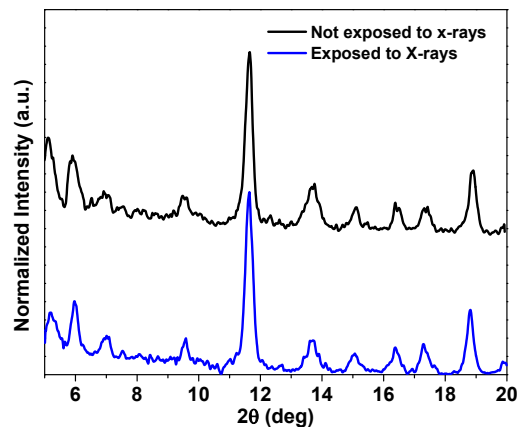
Figure S10. X-ray diffraction patterns of a spot exposed to X-ray beam (blue) and with no exposure (black) confirming integrity of the film after x-ray exposure.

S5. Effect of water co-adsorption on NO adsorbed species

To examine the effect of H_2O incorporation on pre-adsorbed NO, APPES and NEXAFS spectra are collected at a base pressure of 0.03 Torr NO and different added partial pressures of H_2O (Figure S11). The left panel of Figure S11 shows the N 1s XPS spectra at 0.015, 0.07, and 0.17 Torr partial pressure of water (beam exposure times of 230 seconds at each pressure). A decrease in the binding energy of the N 1s peak from 403.5 to 402.8 eV is observed with an increase in H_2O partial pressure. A ~67±2% decrease in the N 1s 403.5 eV peak intensity is observed with an increase of H_2O partial pressure to 0.17 Torr. No change in the area of the peak at 406 eV is observed, indicating a higher affinity of Cu^{1+} to NO as compared to H_2O. The right panel of Figure S11 summarizes the Cu L-edge NEXAFS spectra at a pressure of 0.03 Torr NO, and with addition of 0.17 Torr partial pressure of water. No change in Cu oxidation state is observed. Figure S12 shows the O 1s XPS spectra in UHV and after introducing water vapor.

Pre-exposure of $Cu_3(btc)_2$ to 1 Torr H_2O followed by evacuation and NO adsorption reveals the binding strength of NO at the different adsorption sites (Cu^{2+} and Cu^{1+}). O 1s XPS spectra summarized in Figure S12 at UHV, 0.17, and 0.19 Torr partial pressure of water show a peak at 534 eV assigned to water vapor adsorbed at Cu^{2+}. The reduced intensity of the XPS spectra observed at higher pressures are due to scattering/absorption of the outgoing electrons by the gas. Figure S13 summarizes the normalized integrated areas of the N 1s XPS peaks as a function of NO pressure for an activated versus a hydrated framework (framework pre-exposed to 1 Torr water). While a decrease in the 403.5 eV (peak assigned to NO adsorbed at Cu^{2+}) integrated area is observed for the hydrated as compared to the activated sample. No change in the 406 eV peak area (peak assigned to NO adsorbed at Cu^{1+}) is observed. This result serves as an indication of the stronger bonding of H_2O to Cu^{2+} as compared to Cu^{1+}.
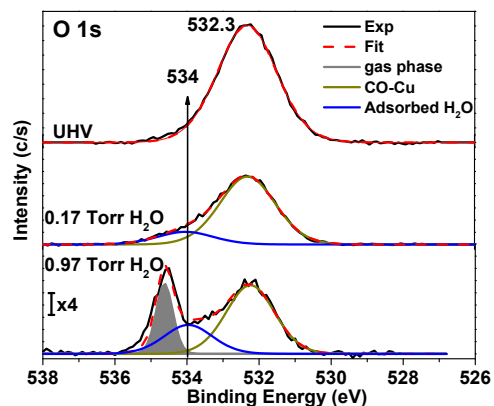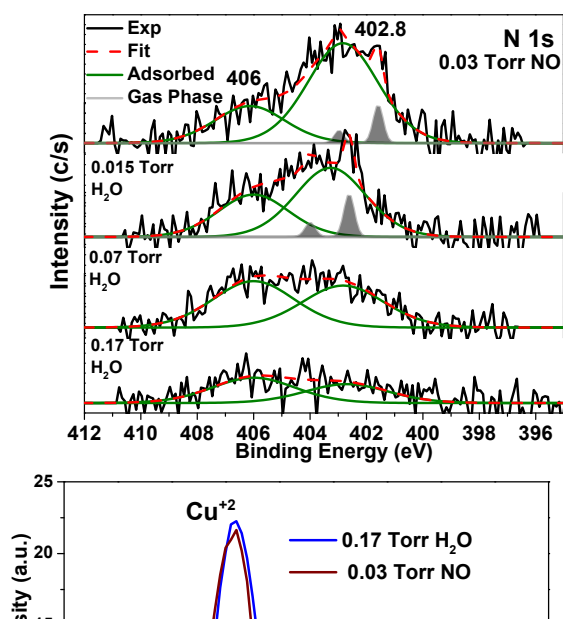
Figure S12. O 1s XPS spectra at UHV (top), 0.17 and 0.97 Torr partial pressure of water. The sharp peak corresponds to gas phase water. The gas pressure affects the intensity of the collected spectra. CO-Cu refers to Cu bonded to COOH of the linker in the framework.
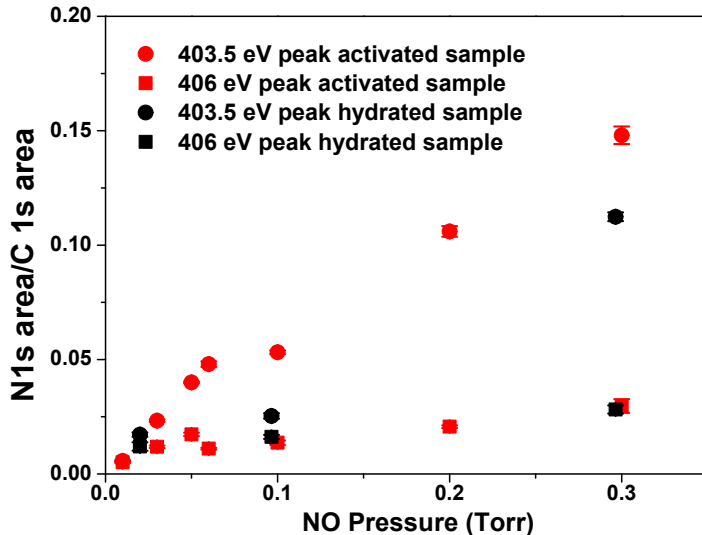
Figure S13. Normalized integrated areas of N 1s core electron peaks as a function of NO pressure for an activated (red symbols)) versus hydrated (black symbols) sample. Uncertainties in estimating the normalized integrated areas are ∼10^{-4}-10^{-3}. ar

S6. Materials and Methods.

Materials Synthesis. $Cu_3(btc)_2$ thin films were synthesized on a SiO_2 substrate using a coated quartz crystal microbalance (QCM) using the Layer by Layer (LBL) method following published methods.[5,7] The SiO_2 coated QCM substrates were cleaned by dipping them into a 2% sodium dedocyl sulfate followed by deionized water rinse then a final step of UV ozone cleaning for 10 minutes. The deposition was performed by flowing a 0.2 mM ethanolic solution of Cu acetate over the functionalized substrate followed by a solvent rinse (ethanol), then flowing a 1 mM ethanolic solution of trimesic acid, followed by another solvent rinse, for a total of 40 layers. Deposition temperature was kept at 22 °C and changes in the frequency and dissipation were simultaneously measured at each layer.

Ambient pressure X-ray photoelectron spectroscopy (APPES). Synchrotron X-ray spectroscopy measurements in the presence of a gas were performed at the Advanced Light Source (ALS) beamline 11.0.2. The experimental setup is described in detail in a paper by Ogletree *et al.* and a review by Bluhm *et al.* [8,9] $Cu_3(btc)_2$ thin film samples were heated overnight in situ at a temperature of 110 °C in ultra-high vacuum using a resistive button heater. A photon energy of 495 eV is used for C 1s core electrons and 600 eV for the N 1s core electrons, 735 eV for O 1s and 1350 eV for Cu 2p; these photon energies provide electrons escaping with a similar energy of 200 eV. An additional set of data for the elements with the same photon energy of 735 eV was collected and used for calibration of peak shifts. NEXAFS spectra were collected in Auger electron yield with a kinetic energy of 750 eV and a kinetic energy bandwidth of 50 eV.

X-ray micro-diffraction measurements.[10] Grazing angle X-ray powder diffraction was employed to identify the synthesized phases. Experiments were performed on the X-ray microdiffraction beamline 12.3.2 at the Advanced Light Source (ALS) of Lawrence Berkeley National Laboratory (LBNL) (Kunz et al, 2009). A vertically focused micro-beam is essential for characterizing thin film synthesis products to maximize the photon interaction within the thin film, rather than the substrate.

The sample was mounted on a chi-stage and the incident angle was optimized such that it was below the critical angle of the gold substrate in order to suppress the gold diffraction signal. This optimization was performed for each sample to maximize sample signal and minimize gold-substrate signal. This procedure was required because the individual sample chips were not parallel within the tolerance of the grazing angle used (<0.5°).

A monochromatic beam of 8047 eV (corresponding to a wavelength of l = 1.5406 Å) was selected from two channel-cut Si(111) monochromator crystals in a dispersive duMont-Hart-Bartels setting. The particular X-ray energy, corresponding to Cu-Ka radiation, was selected to facilitate pattern comparison with literature spectra published at this wavelength.

The X-rays were focused to a spot-size of 1 x 1 um^2 using two dynamically bent X-ray mirrors in Kirkpatrick-Baez arrangement. Powder diffraction patterns were collected with a Pilatus 1M area detector set at a 2q-angle of 42 degrees at a distance of ~150 mm. The X-ray energy was calibrated using the Cu-K-absorption-edge. Detector position (tilt, distance, offset with respect to the incident beam) were calibrated using a powder diffraction pattern of Al_2O_3 placed at the intersection between sample plane and X-ray focal plane using a small depth of field, high-magnification lens, as well as a Keyence laser triangulation system. The same system is employed to subsequently position the samples at the same location. The estimated margin of error for sample positioning is less than 5 um.

The 2-dimensional diffraction patterns were integrated into 1-dimensional intensity vs 2-q patterns using the XMAS program package (Tamura, 2013).[7]

(1)   Petkov, S. P.; Vayssilov, G. N.; Liu, J.; Shekhah, O.; Wang, Y.; Wöll, C.; Heine, T. *Chem. Phys. Chem.* **2012**, *13*, 2025.
(2)   Wu, H.; Chua, Y. S.; Krungleviciute, V.; Tyagi, M.; Chen, P.; Yildirim, T.; Zhou, W. *J. Am. Chem. Soc.* **2013**, *135*, 10525.
(3)   Yang, J.; Regier, T.; Dynes, J. J.; Wang, J.; Shi, J.; Peak, D.; Zhao, Y.; Hu, T.; Chen, Y.; Tse, J. S. *Anal. Chem.* **2011**, *83*, 7856.
(4)   Biesinger, M. C.; Lau, L. W. M.; Gerson, A. R.; Smart, R. S. C. *Applied Surface Science* **2010**, *257*, 887.
(5)   Stavila, V.; Volponi, J.; Katzenmeyer, A. M.; Dixon, M. C.; Allendorf, M. D. *Chem. Sci.* **2012**, *3*, 1531.
(6)   Shekhah, O. *Materials* **2010**, *3*, 1302.
(7)   Liu, B.; Ma, M.; Zacher, D.; Bétard, A.; Yusenko, K.; Metzler-Nolte, N.; Wöll, C.; Fischer, R. A. *J. Am. Chem. Soc.* **2011**, *133*, 1734.
(8)   Frank Ogletree, D.; Bluhm, H.; Hebenstreit, E. D.; Salmeron, M. *Nucl. Instrum. Methods Phys. Res., Sect. A* **2009**, *601*, 151.
(9)   Bluhm, H.; Andersson, K.; Araki, T.; Benzerara, K.; Brown, G. E.; Dynes, J. J.; Ghosal, S.; Gilles, M. K.; Hansen, H. C.; Hemminger, J. C.; Hitchcock, A. P.; Ketteler, G.; Kilcoyne, A. L. D.; Kneedler, E.; Lawrence,

J. R.; Leppard, G. G.; Majzlam, J.; Mun, B. S.; Myneni, S. C. B.; Nilsson, A.; Ogasawara, H.; Ogletree, D. F.; Pecher, K.; Salmeron, M.; Shuh, D. K.; Tonner, B.; Tyliszczak, T.; Warwick, T.; Yoon, T. H. *J. Electron. Spectrosc. Relat. Phenom.* **2006**, *150*, 86.

(10)   Kunz, M.; Tamura, N.; Kai, C.; MacDowell, A. A.; Celestre, R. S.; Church, M. M.; Fakra, S.; Domning, E. E.; Glossinger, J. M.; Kirschman, J. L.; Morrison, G. Y.; Plate, D. W.; Smith, B. V.; Warwick, T.; Yashchuk, V. V.; Padmore, H. A.; Ustundag, E. *Rev. Sci. Instrum.* **2009**, *80*, 035108.